

# Data visualization and dimension reduction for metric-valued response regression

Abdul-Nasah Soale\*

Department of Mathematics, Applied Mathematics, and Statistics  
Case Western Reserve University, Cleveland, OH, USA

and

Yuexiao Dong

Department of Statistics, Operations, and Data Science  
Temple University, Philadelphia, PA, USA

October 20, 2023

## Abstract

As novel data collection becomes increasingly common, traditional dimension reduction and data visualization techniques are becoming inadequate to analyze these complex data. A surrogate-assisted sufficient dimension reduction (SDR) method for regression with a general metric-valued response on Euclidean predictors is proposed. The response objects are mapped to a real-valued distance matrix using an appropriate metric and then projected onto a large sample of random unit vectors to obtain scalar-valued surrogate responses. An ensemble estimate of the subspaces for the regression of the surrogate responses versus the predictor is used to estimate the original central space. Under this framework, classical SDR methods such as ordinary least squares and sliced inverse regression are extended. The surrogate-assisted method applies to responses on compact metric spaces including but not limited to Euclidean, distributional, and functional. An extensive simulation experiment demonstrates the superior performance of the proposed surrogate-assisted method on synthetic data compared to existing competing methods where applicable. The analysis of the distributions and functional trajectories of county-level COVID-19 transmission rates in the U.S. as a function of demographic characteristics is also provided. The theoretical justifications are included as well.

*Keywords:* dimension reduction, Fréchet regression, non-Euclidean response, Wasserstein distance, COVID-19 transmission

---

\*Corresponding author: [abdul-nasah.soale@case.edu](mailto:abdul-nasah.soale@case.edu)

# 1 Introduction

Lately, there has been a growing interest in statistical applications on novel data sets where the traditional regression framework cannot be extended. Although the regression methodology has been expanded to accommodate complex data types such as manifolds, there are some metric spaces with little or no algebraic structure that are difficult to model using the existing methodology. These metric spaces include the space of probability distributions, covariance matrices, images, and shapes, to mention a few. Some examples of applications in such metric spaces can be seen in Faraway (2014), Petersen & Müller (2019), Bhattacharjee & Müller (2021), and Ghosal et al. (2023). While inner products, norms, and other operations on a vector space do not apply in these metric spaces, we can compute the distance between the objects. Therefore, Faraway (2014) proposed to first compute scores of the pairwise distance matrix of the response and the predictor and then apply a classical regression on the scores. The scores can be transformed back to the original metric space using a back-scoring technique. Recently, Petersen & Müller (2019) also proposed Fréchet regression for the case where only the responses are allowed to be on a general metric space but the predictors are Euclidean. We focus our attention on the latter.

Fréchet regression basically extends the Fréchet mean of Fréchet (1948) to the conditional Fréchet mean. That is, for a random response object  $Y$  in a metric space  $(\Omega_Y, d)$  equipped with a metric  $d$ , let  $\mathbf{X} \in \mathbb{R}^p$  be a  $p$ -dimensional predictor with  $F_X$  and  $F_Y$  denoting the marginal distributions of  $\mathbf{X}$  and  $Y$ , respectively. Also, let  $(\mathbf{X}, Y)$  be a random object on the product space  $\mathbb{R}^p \times \Omega_Y$  with a joint distribution function given by  $F_{XY}$ , and assume the conditional distributions  $F_{X|Y}$  and  $F_{Y|X}$  exist and are well-defined. The Fréchet regression function of  $Y$  given  $\mathbf{X}$  is defined by Petersen & Müller (2019) as

$$m_{\oplus}(\mathbf{x}) = \arg \min_{\omega \in \Omega_Y} M_{\oplus}(., \mathbf{x}),$$

where the conditional Fréchet function  $M_{\oplus}(., \mathbf{x}) = \mathbb{E}[d^2(Y, .) | \mathbf{X} = \mathbf{x}]$ .

It is not hard to see that like the traditional regression setting, Fréchet regression also suffers from the curse of dimensionality as  $p$  becomes large. This motivated the development of Fréchet dimension reduction which extends existing traditional sufficient dimension reduction (SDR) methods to random response objects in non-Euclidean metric spaces such as probability distributions, symmetric positive definite matrices, and spheres. See Zhang et al. (2021) and Dong & Wu (2022) for examples. The goal of the Fréchet SDR is to find the smallest set of linear combinations of  $\mathbf{X}$ , which captures the relevant information in  $\mathbf{X}$  needed to predict  $Y$  without loss of information. Thus, the Fréchet dimension reduction subspace  $\mathcal{S}$  is such that

$$Y \perp\!\!\!\perp \mathbf{X} | \mathbf{P}_{\mathcal{S}} \mathbf{X}, \quad (1)$$

where “ $\perp\!\!\!\perp$ ” means statistical independence and  $\mathbf{P}_{\mathcal{S}}$  denotes the projection onto  $\mathcal{S}$  with respect to the inner product in  $\mathbb{R}^p$ . Cook (1996) and Yin et al. (2008) can be extended to show that under some mild conditions, a unique  $\mathcal{S}$  with the smallest column space exists, and it is called the Fréchet central space for the regression of  $Y$  on  $\mathbf{X}$ , denoted as  $\mathcal{S}_{Y|\mathbf{X}}$ . Therefore, if an orthogonal matrix  $\mathbf{B} \in \mathbb{R}^{p \times d}$  with  $d < p$  is such that  $\mathbf{B}^\top \mathbf{B} = \mathbf{I}_d$  and  $\text{span}(\mathbf{B}) = \mathcal{S}_{Y|\mathbf{X}}$ , then  $\mathbf{B}$  is a basis for  $\mathcal{S}_{Y|\mathbf{X}}$ , where  $\mathbf{I}_d$  denotes a  $d \times d$  identity matrix and  $\text{span}(\cdot)$  denotes the column space. Lastly,  $\dim(\mathcal{S}_{Y|\mathbf{X}}) = d$  is called the structural dimension.

Both Zhang et al. (2021) and Dong & Wu (2022) proposed to use universal kernels  $\kappa : \Omega_Y \times \Omega_Y \rightarrow \mathbb{R}$  to estimate the central space. For a compact response space  $(\Omega_Y, d)$ , a universal kernel on  $\Omega_Y$  can be defined as the continuous kernel on  $\Omega_Y$  such that the reproducing kernel Hilbert space generated by this kernel is dense in  $C(\Omega_Y)$ , where  $C(\Omega_Y)$  is the family of continuous real-valued functions on  $\Omega_Y$ . Notice that while the continuous embedding conditions cover several instances, it limits our choice of kernels. For instance, in general metric spaces, the Gaussian radial basis kernel is not guaranteed to be universal. Moreover, even after choosing the right kernel, we still have to worry about determining the optimal tuning parameters. Besides, the computational cost that comes with computing

these high-dimensional kernels can be expensive.

To avoid these problems, we follow in the spirit of Faraway (2014). First, we find the pairwise distance matrix between the response objects, which we use to represent the original response. By the transformational properties of the central space (see Theorem 2.3 of Li (2018)), we can estimate a direction(s) in the central space using the transformed response. To this end, the high dimensionality of the distance matrix, especially in large samples is addressed using scalar projections of the distance matrix. We call the new scalar mappings of the distance matrix the surrogate responses. With the surrogate response, we proceed to implement a traditional SDR technique to estimate the subspace for the sampled projected response. This way, we avoid generating high-dimensional kernels and simplify the estimation in finite samples. Our proposal provides a unified framework for handling responses in general compact metric spaces encompassing responses in both Euclidean and non-Euclidean spaces. While there is little or no incentive to use the surrogate method in the classical Euclidean setting, the surrogate technique is especially useful when heteroscedasticity is present. We illustrate this in the toy example that follows.

## 1.1 Motivating example

To fix the idea of surrogate-assisted SDR, we consider a toy example with a scalar response in Euclidean space, where there is little or no incentive to use this technique. We formulate the toy example as follows. Fix a random sample of size  $n = 100$  and generate a predictor  $\mathbf{X} \sim N(\mathbf{0}, \mathbf{I}_2)$ . Next, generate the response as

$$Y = (1 + \beta_0^\top \mathbf{X})\epsilon, \quad (2)$$

where  $\beta_0^\top = (1, 1)$  and  $\epsilon \sim N(0, 0.5^2)$ . As  $Y$  follows a normal distribution with zero mean and non-constant variance, classical methods like the ordinary least squares (OLS) will not be able to recover  $\beta_0$  because the central mean space  $\mathcal{S}_{E(Y|\mathbf{X})} = \{\mathbf{0}\}$ . The scatter plots of  $Y$  versus  $X_1$  and  $X_2$  are given in Figure 1.

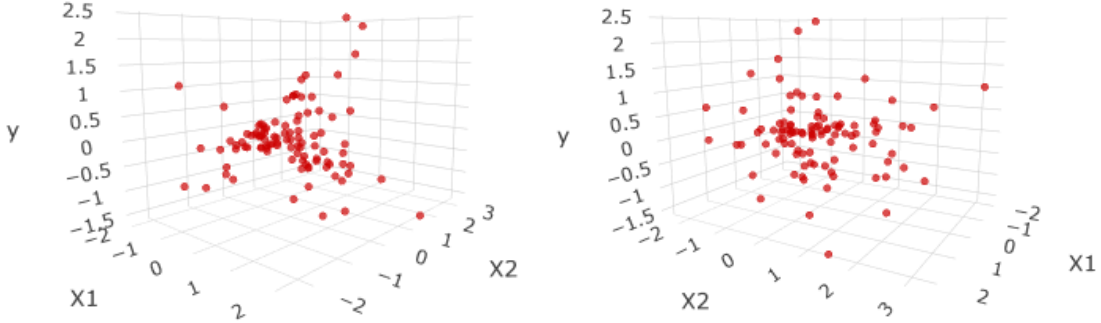


Figure 1: 3D scatter plots of  $Y$  versus the  $X_1$  and  $X_2$  from the direction of  $X_1$  (left) and  $X_2$  (right).

It is important to note that although  $Y$  depends on  $\mathbf{X}$  only through the variance, the absolute difference between any response pair  $(Y_i, Y_j)$  depends on  $\mathbf{X}$  through both the mean and the variance. Because  $Y_i - Y_j \sim N(0, 0.5^2[(1 + \beta_0^\top \mathbf{X}_i)^2 + (1 + \beta_0^\top \mathbf{X}_j)^2])$ , we have  $|Y_i - Y_j|$  as a folded normal distribution given by

$$|Y_i - Y_j| \sim FN(\mu_Y, \sigma_Y^2), \quad i, j = 1, \dots, n,$$

$$\text{where } \mu_Y = \frac{0.5\sqrt{2[(1 + \beta_0^\top \mathbf{X}_i)^2 + (1 + \beta_0^\top \mathbf{X}_j)^2]}}{\sqrt{\pi}} \text{ and } \sigma_Y^2 = 0.5^2[(1 + \beta_0^\top \mathbf{X}_i)^2 + (1 + \beta_0^\top \mathbf{X}_j)^2].$$

We proceed to estimate  $\beta_0$  using OLS and surrogate-assisted OLS (sa-OLS). The OLS estimate of  $\beta_0$  is  $(0.023, -0.04)$  while the sa-OLS estimate is  $(0.94, 0.70)$ . The estimation of sa-OLS is discussed later in Section 3.5. We see clearly that while OLS struggles to recover any direction in the mean space, sa-OLS recovers a direction that is very close to the truth. The underlying structure based on the true and estimated directions is given in Figure 2.

The rest of the paper is organized as follows. In Section 2, we describe the mapping between metric spaces and how it relates to the central space at the population level. The sample estimation and the properties of the estimates are discussed in Section 3. The performance of our proposed surrogate-assisted techniques compared to existing methods on synthetic and real data are provided in Sections 4 and 5, respectively. The paper concludes with a discussion in Section 6. All proofs are relegated to the appendix.

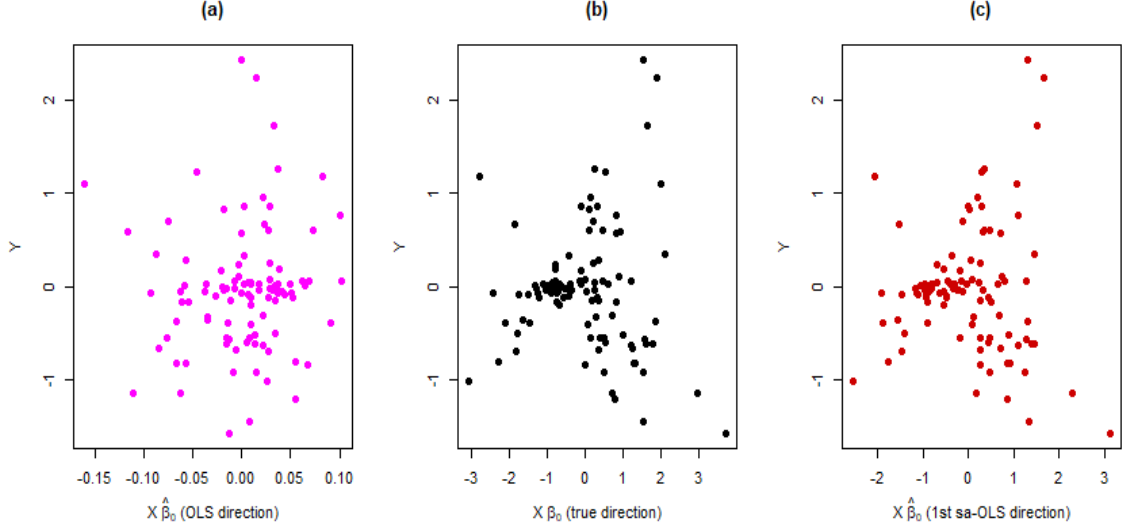


Figure 2: Comparison between the true direction and the estimated directions based on ordinary least squares (OLS) and surrogate-assisted OLS (sa-OLS)

## 2 Metric embedding and the central space

### 2.1 Metric mapping

Consider a mapping from  $\mathbb{R}^p$  to a general metric space  $(\Omega_Y, d)$  given by

$$f : \mathbb{R}^p \rightarrow (\Omega_Y, d).$$

We allow the mapping  $f$  to have some distortions so that for any  $(\mathbf{X}, Y) \in (\mathbb{R}^p \times \Omega_Y)$ , we assume that

$$Y = f(\mathbf{X}) + \epsilon, \quad (3)$$

where  $f$  is unknown and the error  $\epsilon$  is such that  $E(\epsilon|\mathbf{X}) = 0$  almost surely. Assume  $f$  is an injective mapping and suppose for some  $\gamma \geq 1$ , there exists an  $r > 0$  such that

$$r\|\mathbf{X} - \mathbf{X}'\| \leq d_Y(f(\mathbf{X}), f(\mathbf{X}')) \leq \gamma r\|\mathbf{X} - \mathbf{X}'\|,$$

where  $(\mathbf{X}, \mathbf{X}') \in \mathbb{R}^p$ . Then, we call  $f$  a  $\gamma$ -embedding.

**Definition 1** (Spread at a point; Wilson (1935)). *Let  $Y = f(\mathbf{X})$  be a scalar transformation. For any  $(\mathbf{X}, \mathbf{X}') \in \mathbb{R}^p$  with corresponding images as  $(Y, Y') \in \Omega_Y$ , let  $d_X = \|\mathbf{X} - \mathbf{X}'\|$  and  $d_Y = d(Y, Y')$ . Then for any limiting point  $\mathbf{X}_0$  of  $\mathbb{R}^p$ , the spread at  $\mathbf{X}_0$  is given by  $s_f(\mathbf{X}_0) = \lim d_Y/d_X$  as  $\mathbf{X}$  and  $\mathbf{X}'$  approach  $\mathbf{X}_0$ . Thus,  $s_f(\mathbf{X}_0)$  can be finite, infinite, or indeterminate.*

Following definition 1, assume  $d_Y = \phi(d_X)$ , where  $\phi(\cdot)$  is a scalar-valued function that satisfies the following properties:

- i.  $\phi(d_X) > 0$  if  $d_X > 0$ ;
- ii.  $\phi(d_X) = 0$  if  $d_X = 0$ ;
- iii.  $\phi(d_X)$  is continuous;
- iv.  $d_{X_1} + d_{X_2} \geq d_{X_3}$  implies  $\phi(d_{X_1}) + \phi(d_{X_2}) \geq \phi(d_{X_3})$ .

Then  $Y = f(\mathbf{X})$  is an *unrestricted transformation* as it can be applied to any metric space, and the transformation is *regular* because it has a constant spread. Such a transformation preserves congruence and applies to some subspace of  $\mathbb{R}^p$  even if  $\phi(d_X)$  satisfies only (i), (ii), and (iii) but not (iv). This means  $Y$  can belong to any bounded metric space as long as the transformation is monotone and continuous in  $\mathbb{R}^p$  with a finite spread at each point.

**Theorem 1.** *Assume  $\mathcal{X} = \{\mathbf{X}\} \subset \mathbb{R}^p$  and  $\Omega_Y$  are compact and let  $(\mathbf{X}, Y)$  and  $(\mathbf{X}', Y')$  be any two points in  $\mathcal{X} \times \Omega_Y$ .*

- (a) *If  $Y = f(\mathbf{X})$  is a continuous transformation with a finite spread at each limiting point of  $\mathbb{R}^p$ , then  $d_Y/d_X$  is bounded in  $\mathbb{R}^p$ .*
- (b) *If  $Y = f(\mathbf{X})$  is a transformation with a finite spread that is continuous in  $\mathbb{R}^p$ , then  $d_Y/d_X$  converges to  $s_f(\mathbf{X})$  uniformly in  $\mathbb{R}^p$ .*

## 2.2 Central space for metric response regression

For a surface  $S \in \mathbb{R}^p$ , the central space is the direction in  $\mathbb{R}^p$  with the most change in the height of  $S$ , which also aligns with the gradient direction of  $S$ . Therefore, following Theorem 1, if we restrict  $f(\cdot)$  to continuous monotone functions, the gradient direction will always exist and can be used to estimate the central space. Next, by the definition of sufficient dimension reduction in (1), if we let  $\tilde{Y}$  be a random copy of  $Y$ , then we have

$$(Y, \tilde{Y}) \perp\!\!\!\perp \mathbf{X} | \mathbf{P}_S \mathbf{X} \implies \psi(Y, \tilde{Y}) \perp\!\!\!\perp \mathbf{X} | \mathbf{P}_S \mathbf{X}, \quad (4)$$

for any measurable function  $\psi$ . The relationship in (4) implies that we can recover  $\mathcal{S}_{Y|\mathbf{X}}$  from the subspaces of the regression of  $\psi(Y, \tilde{Y})$  on  $\mathbf{X}$ . We refer to the new response  $\psi(Y, \tilde{Y})$  as the surrogate response, denoted as  $Y^s$ .

**Lemma 1.** *For any measurable function  $\psi$ ,  $\mathcal{S}_{Y^s|\mathbf{X}} \subseteq \mathcal{S}_{Y|\mathbf{X}}$ .*

Lemma 1 implies that  $\mathcal{S}_{Y|\mathbf{X}}$  can be characterized using the collection of subspaces for the regression of  $Y^s$  versus  $\mathbf{X}$  by borrowing the ensemble idea of Yin & Li (2011).

**Definition 2.** *Let  $\xi$  be a family of functions  $\psi : \Omega_Y \rightarrow \mathbb{R}$ . Then  $\xi$  characterizes  $\mathcal{S}_{Y|\mathbf{X}}$  if*

$$\begin{aligned} (a) \quad & \text{span}\{\mathcal{S}_{E(Y^s|\mathbf{X})} : \psi \in \xi\} = \mathcal{S}_{Y|\mathbf{X}}, \\ (b) \quad & \text{span}\{\mathcal{S}_{Y^s|\mathbf{X}} : \psi \in \xi\} = \mathcal{S}_{Y|\mathbf{X}}. \end{aligned} \quad (5)$$

Part (a) of (5) is called the central mean space (CMS) ensemble while (b) is referred to as the central space (CS) ensemble. We denote either the CMS or CS ensemble for  $\psi \in \xi$  as  $\mathcal{S}(\xi)$ .

The next Lemma is a modification of the results in Yin & Li (2011). We note that for the CMS based on first-order methods such as OLS, we only require the first moment of the class of functions of  $Y^s$  to exist. However, to accommodate other methods for estimating the central space, we require the class of functions of  $Y^s$  to be square integrable, which indirectly satisfies that the first moment of the functions exists.

**Lemma 2.** Let  $L_2(F_Y)$  be the class of square-integrable functions of  $Y^s$  and  $\mathcal{I}$  be a class of measurable indicator functions of  $Y^s$ . If  $\xi \subseteq L_1(F_Y) = \{\psi : E|\psi(\Omega_Y)| < \infty\}$  is a subset of the class of functions with finite first moment, then

- (a)  $\mathcal{S}(\xi) \subseteq \mathcal{S}_{Y|\mathbf{X}}$ .
- (b)  $\mathcal{S}(\xi) \supseteq \mathcal{S}_{Y|\mathbf{X}}$  if  $E(Y|\mathbf{X}) = E(Y^s|\mathbf{P}_{\mathcal{S}}\mathbf{X})$  for all  $\psi \in \xi$ .
- (c) suppose  $L_2(F_Y)$  is dense in  $\mathcal{I}$  and  $\xi \subseteq L_2(F_Y)$ , then  $\xi$  characterizes the  $\mathcal{S}_{Y|\mathbf{X}}$  as well.

Because  $Y^s$  is a scalar, if  $f(\cdot)$  is a monotone link, Lemma 2 implies that we can easily employ traditional SDR methods like OLS and SIR for the CMS and CS ensembles, respectively. More specifically, Lemma 2 (b) shows that consistent and exhaustive estimates of  $\mathcal{S}_{Y|\mathbf{X}}$  can be achieved if  $E(Y|\mathbf{X}) = E(Y^s|\mathbf{P}_{\mathcal{S}}\mathbf{X})$  for all  $\psi \in \xi$ .

Typically, for the ensemble estimate of the central space, we find a candidate matrix  $\mathbf{M} : P_{XY} \times \xi \rightarrow \mathbb{R}^{p \times p}$  such that  $\text{Span}(\mathbf{M}) \subseteq \mathcal{S}_{Y|\mathbf{X}}$ , where  $P_{XY} = \{F_{XY}\}$  is a collection of all distributions of  $(\mathbf{X}, Y)$ . For the classical OLS and SIR, we require the linear conditional mean (LCM) assumption, which assumes that  $E(\mathbf{X}|\mathbf{B}^\top \mathbf{X})$  is a linear function of  $\mathbf{B}^\top \mathbf{X}$  if  $\mathbf{B}$  is a basis of  $\mathcal{S}_{Y|\mathbf{X}}$ . Since the LCM is a requirement on only the predictor, it is still required for the surrogate-assisted OLS and SIR.

Suppose  $\mathbf{X}$  satisfies the LCM assumption and  $\Sigma = \text{Var}(\mathbf{X})$  is nonsingular. For any  $\psi \in \xi$ , the sa-OLS estimator is given by  $\beta(\psi) = \Sigma^{-1} \Sigma_{XY^s} \in \mathcal{S}_{Y|\mathbf{X}}$ , where  $\Sigma_{XY^s}$  denotes the covariance between  $\mathbf{X}$  and  $Y^s$ . As a consequence,  $\mathbf{M}_{ols} = E[\beta(\psi)\beta^\top(\psi)]$  is a candidate matrix for estimating  $\mathcal{S}_{Y|\mathbf{X}}$ , where the expectation is taken over all  $\psi \in \xi$ . It is important to note that, unlike the classical OLS, sa-OLS can estimate more than one direction in the central space. Moreover, as demonstrated in the toy example, sa-OLS can handle heteroscedastic errors and models with monotone links where  $E(Y|\mathbf{X}) = 0$ . Similarly, the candidate matrix for the sa-SIR estimator is given by  $\mathbf{M}_{sir}(\cdot, \psi) = E\{ \text{Var}[E(\mathbf{X}|Y^s)] \}$ , where the outer expectation  $E\{\cdot\}$  is taken over all  $\psi \in \xi$ .

### 3 Estimation in finite sample

Let  $(\mathbf{x}_1, y_1), \dots, (\mathbf{x}_n, y_n)$  be a random sample of  $(\mathbf{X}, Y)$ . We define  $Y^s = u^\top \mathbf{D}_n$ , where  $\mathbf{D}_n$  is a matrix of pairwise distances  $(y_i, y_j)$ ,  $i, j = 1, \dots, n$  and  $u \in \mathbb{R}^n$  with  $\|u\| = 1$ . The key thing is to use the appropriate metric to estimate the distance matrix. We illustrate this for response in three different metric spaces.

#### 3.1 Euclidean responses

Let  $Y_n = \{y_1, \dots, y_n\} \in \mathbb{R}^q$ , where  $q \geq 1$ . For  $q = 1$ , we estimate the pairwise distances as the absolute difference between any two points in the set. That is,  $\mathbf{D}_n[ij] = |y_i - y_j|, \forall i, j = 1, \dots, n$ . On the other hand, if  $q > 1$ , then we may use the  $\ell_2$ -norm:  $\mathbf{D}_n[ij] = [\sum_{k=1}^q (y_{ik} - y_{jk})^2]^{1/2}$ . Other distance functions that satisfy the properties of a metric such as the Mahalanobis distance may also be used.

#### 3.2 Distributional responses

For response objects that are probability distributions, we propose to use the Wasserstein metric. In lay terms, Wasserstein distance measures the minimum amount of work required to transform one distribution into another. Let  $\zeta$  and  $\nu$  be probability measures on  $\mathbb{R}^q$  with finite  $k$ th moment. The  $k$ -Wasserstein distance is defined as

$$W_k(\zeta, \nu) = \inf_{\substack{y \sim \zeta \\ y' \sim \nu}} (\mathbb{E} \|y - y'\|_k)^{1/k}, \quad k \geq 1, \quad (6)$$

where  $\|\cdot\|_k$  is the  $\ell_k$ -norm with the infimum taken over all pairs of  $(y, y') \in \mathbb{R}^q$  with  $y$  and  $y'$  marginally distributed as  $\zeta$  and  $\nu$ , respectively (Panaretos & Zemel (2019)). For univariate distributions,  $W_k(\cdot)$  has an explicit definition.

Let  $y_1, y_2$  be probability measures on  $\mathbb{R}$  with cumulative distribution functions  $F_{y_1}$  and  $F_{y_2}$ , respectively. Suppose the  $k$ th moments of  $y_1$  and  $y_2$  exist, then the  $k$ -Wasserstein

distance is explicitly defined as

$$W_k(y_1, y_2) = \|F_{y_1}^{-1} - F_{y_2}^{-1}\|_k = \left( \int_0^1 |F_{y_1}^{-1}(s) - F_{y_2}^{-1}(s)|^k ds \right)^{1/k}, \quad (7)$$

where  $F_{y_1}^{-1}$  and  $F_{y_2}^{-1}$  are the respective quantile functions of  $y_1$  and  $y_2$ . Specifically, for  $k = 2$ , equation (7) implies that

$$W_2^2(y_1, y_2) = W_2^2(y_1^*, y_2^*) + (\mu_1 - \mu_2)^2,$$

where  $\mu_1$  and  $\mu_2$  are the respective means of  $y_1$  and  $y_2$ , and  $y_1^*$  and  $y_2^*$  are the respective mean centered translations of distributions  $y_1$  and  $y_2$ . In the special case where  $y_1 \sim N(\mu_1, \sigma_1^2)$  and  $y_2 \sim N(\mu_2, \sigma_2^2)$ ,  $W_2(y_1, y_2) \geq |\mu_1 - \mu_2|$ .

### 3.3 Functional responses

Here, we focus on responses measured over time but not necessarily at fixed time intervals. Our metric of choice is one that takes into account both the phase and amplitude variations. Faraway (2014) proposed to use the Fréchet distance. We choose to follow the technique of Agrawal et al. (1993), which basically uses the discrete Fourier transform (DFT) to map the response sequence to the frequency domain to reveal the periodicities and their relative strengths at the periodic components, and then compute the Euclidean distance between the modulus of the Fourier coefficients.

Let  $y(t)$  denote the functional response measured at time (sample)  $t = 1, \dots, T$ . The DFT of  $y(t)$  is a sequence of complex numbers of the same length  $T$  given by

$$Y(k) = \sum_{t=0}^{T-1} y(t) e^{-i2\pi kt/T}, k = 0, 1, 2, \dots, T-1, \quad (8)$$

where  $Y(k)$  denotes the  $k$ th spectral sample and  $i = \sqrt{-1}$  is the imaginary unit. The advantage of the DFT is that we can reconstruct the original sequence as follows:

$$y(t) = \frac{1}{T} \sum_{k=0}^{T-1} Y(k) e^{i2\pi kt/T}, k = 0, 1, 2, \dots, T-1. \quad (9)$$

By Parseval’s theorem, the Fourier transform preserves the Euclidean distance in both the time and frequency domains. Thus, we can find the distance between any two functional responses by calculating the Euclidean distance between the modulus of their Fourier coefficients. The Fourier transform maps the sequence to a low-dimensional space using only the first few Fourier coefficients, which means we do not need all the coefficients to reconstruct the original sequence. Thus, we use  $\lfloor T/2 \rfloor + 1$  coefficients as used in the *TSdist* package in *R* (Mori et al. (2016)).

### 3.4 Distance matrix as high dimensional response

Once we represent  $Y_n = \{y_1, \dots, y_n\}$  as a pairwise distance matrix  $\mathbf{D}_n$ , we transform the problem to a traditional multivariate response SDR regardless of the original space of  $Y$ . Therefore, theoretically, we can proceed to apply SDR techniques such as OLS and SIR. However, it is clear in the multivariate response SDR literature that smoothing over high dimensions easily suffers from the curse of dimensionality. Thus, several techniques to overcome this high-dimensional problem have been proposed. See Dong et al. (2022) for a selective review. We adopt the projective resampling technique of Li et al. (2008) which has been shown to have good asymptotic properties.

Our choice of the projective resampling technique can also be justified directly from the Johnson-Lindenstrauss Lemma. Moreover, as Huber (1985) noted, any high dimensional random vector can be characterized by its univariate projection as can be seen trivially by the property of characteristic functions of random vectors. That is,  $\psi_{u^\top \mathbf{D}_n}(t) = \mathbb{E}(e^{it^\top u^\top \mathbf{D}_n}) = \psi_{\mathbf{D}_n}(ut)$ , which means the characteristic function of the 1-dimensional projection of  $\mathbf{D}_n$  onto any vector  $u$ , equals the section of the characteristic function of  $\mathbf{D}_n$  along  $u$ . Because  $u$  is randomly chosen, we estimate the subspaces for several unit vectors using OLS or SIR and average them to estimate  $\mathcal{S}_{Y|\mathbf{X}}$ .

### 3.5 Estimation algorithms

For ease of computation, we typically estimate the candidate matrix based on a standardized predictor  $\mathbf{Z} = \Sigma^{-1/2}(\mathbf{X} - \boldsymbol{\mu})$ , where  $\boldsymbol{\mu}$  and  $\Sigma$  denote the mean and covariance of  $\mathbf{X}$ , respectively. By the invariance property of the central space, if  $\mathbf{M}$  is the candidate matrix for  $Y$  versus  $\mathbf{Z}$ , then  $\Sigma^{-1/2}\text{Span}(\mathbf{M}) \in \mathcal{S}_{Y|\mathbf{X}}$ . The sa-OLS and sa-SIR algorithms are given below.

---

**Algorithm 1** sa-OLS

---

- 1: Input: Predictor  $\mathbf{X}$  as  $(n \times p)$  matrix, response  $Y_n = \{y_1, \dots, y_n\}$  as list
- 2: Define:  $n \times n$  matrix  $\mathbf{D}_n$ ,  $\mathbf{D}_n[i, j] \leftarrow d(y_i, y_j)$ ,  $\forall i, j = 1 \dots, n$
- 3: Compute:  $\bar{\mathbf{x}} = n^{-1} \sum_{i=1}^n \mathbf{x}_i$ ,  $\hat{\Sigma} = n^{-1}(\mathbf{x}_i - \bar{\mathbf{x}})(\mathbf{x}_i - \bar{\mathbf{x}})^\top$ , and  $\hat{\mathbf{z}} \leftarrow \hat{\Sigma}^{-1/2}(\mathbf{x} - \bar{\mathbf{x}})$
- 4: Set:  $N \leftarrow$  large integer ( $\geq 1000$ )
- 5: **for** each  $k$  in  $1, \dots, N$  **do**
- 6:      $u_k \leftarrow U/\|U\|$ ,  $U \sim N(0, 1)$
- 7:      $y_k^s \leftarrow u_k^\top \mathbf{D}_n$
- 8:      $\hat{\boldsymbol{\beta}}(u_k) \leftarrow \hat{\Sigma}^{-1} \hat{\Sigma}_{zy_k^s}$ ,  $\hat{\Sigma}_{zy_k^s} = \text{Cov}(\hat{\mathbf{z}}, y_k^s)$
- 9:      $\mathbf{M}_k \leftarrow \hat{\boldsymbol{\beta}}(u_k) \hat{\boldsymbol{\beta}}(u_k)^\top$
- 10: **end for**
- 11: Compute:  $\mathbf{M}_{ols} \leftarrow N^{-1} \sum_{k=1}^N \mathbf{M}_k$
- 12: Return:  $\hat{\mathbf{B}} = \hat{\Sigma}^{-1/2}(\hat{\mathbf{v}}_1, \dots, \hat{\mathbf{v}}_d)$ , where  $(\hat{\mathbf{v}}_1, \dots, \hat{\mathbf{v}}_d)$  are the eigenvectors corresponding to the  $d$  leading eigenvalues of  $\hat{\mathbf{M}}_{ols}$ .

---

---

**Algorithm 2** sa-SIR

---

1: Repeat: 1-4 of Algorithm 1

2: **for** each  $k$  in  $1, \dots, N$  **do**

3:      $u_k \leftarrow U/\|U\|$ ,  $U \sim N(0, 1)$

4:      $y_k^s \leftarrow u_k^\top \mathbf{D}_n$

5:     partition  $supp(y_k^s)$  into intervals  $I_1(u_k), \dots, I_H(u_k)$ .

6:     Set:  $I_{hi}(u_k) \leftarrow \mathbf{I}(y_k^s \in I_h(u_k))$

7:      $\hat{p}_h(u_k) \leftarrow n^{-1} \sum_{i=1}^n I_{hi}(u_k)$

8:      $\hat{\mu}_h(u_k) \leftarrow \{n\hat{p}_h(u_k)\}^{-1} \sum_{i=1}^n \hat{z}_i I_{hi}(u_k)$

9:      $\mathbf{M}_k \leftarrow \sum_{h=1}^H \hat{p}_h(u_k) \hat{\mu}_h(u_k) \hat{\mu}_h^\top(u_k)$

10: **end for**

11: Compute:  $\mathbf{M}_{sir} \leftarrow N^{-1} \sum_{k=1}^N \mathbf{M}_k$

12: Return:  $\hat{\mathbf{B}} = \hat{\Sigma}^{-1/2}(\hat{\mathbf{v}}_1, \dots, \hat{\mathbf{v}}_d)$ , where  $(\hat{\mathbf{v}}_1, \dots, \hat{\mathbf{v}}_d)$  are the eigenvectors corresponding to the  $d$  leading eigenvalues of  $\hat{\mathbf{M}}_{sir}$ .

---

The procedure in Algorithm 2 can be followed to estimate the candidate matrix for methods not covered here such as directional regression.

### 3.6 Properties of the sample estimator

Li et al. (2008) already established the asymptotic properties of the projective resampling SDR estimators for regressing multivariate responses  $\mathbf{Y} \in \mathbb{R}^q$ ,  $q \geq 2$  on  $\mathbf{X} \in \mathbb{R}^p$ . The same approach can be adopted to establish the asymptotic properties of the surrogate-assisted SDR methods by replacing  $Y$  with  $\mathbf{D}_n$ .

For a uniformly distributed random vector  $U \in \mathbb{S}^{n-1}$ , let  $\mathbf{M}(U)$  be such that  $\text{Span}(\mathbf{E}[\mathbf{M}(U)]) \subseteq \mathcal{S}_{Y|\mathbf{X}}$ . Let  $\mathbf{M}_n(\mathbf{U}_N) = N^{-1} \sum_{i=1}^N \mathbf{M}_n(u_i)$  be the sample estimate of  $\mathbf{E}[\mathbf{M}(U)]$  as described in Section 3.5 based on the sample unit vectors  $\mathbf{U}_N = \{u_1, \dots, u_N\} \in \mathbb{S}^{n-1}$ . Each  $\mathbf{M}_n(u_i)$

is positive semidefinite and by the weak law of large numbers  $\mathbf{M}_n(\mathbf{U}_N) \xrightarrow{p} \mathbf{E}[\mathbf{M}(\mathbf{U})]$  if we choose  $N$  to be large enough. Assume also that for any  $u$  the following first-order expansion of  $\mathbf{M}_n(u)$  hold:

$$\mathbf{M}_n(u) = \mathbf{M}(u) + \mathbf{E}_n[\Psi(\mathbf{X}, \mathbf{D}_n, u)] + \mathbf{R}_n(u), \quad (10)$$

where  $\Psi(\mathbf{X}, \mathbf{D}_n, u)$  is some square integrable function with zero mean and  $\mathbf{R}_n(u)$  is a remainder with  $\sup_{u \in \mathbb{S}^{n-1}} \|\mathbf{R}_n(u)\|_F = o_p(n^{-1/2})$ .

Suppose these conditions are satisfied, the following theorem establishes the  $\sqrt{n}$  consistency and asymptotic normality of the estimator.

**Theorem 2.**

Suppose  $n = O(N)$  and  $\mathbf{U}_N = (u_1, \dots, u_N)$ , then

$$\mathbf{M}_n(\mathbf{U}_N) = \mathbf{E}[\mathbf{M}(\mathbf{U})] + O_p(n^{-1/2}), \quad (11)$$

$$\sqrt{n} \{ \mathbf{M}_n(\mathbf{U}_N) - \mathbf{E}[\mathbf{M}(\mathbf{U})] \} \xrightarrow{d} N(\mathbf{0}, \mathbf{C}), \text{ if } \lim_{n \rightarrow \infty} (n/N) = 0, \quad (12)$$

where  $\mathbf{M}_n(\mathbf{U}_N)$  is the sample estimate of  $\mathbf{M}(\mathbf{U})$  based on  $N$  random unit vectors  $u_1, \dots, u_N$  and  $\mathbf{C}$  is some positive definite matrix.

By theorem 2, the sample estimator for  $\mathcal{S}_{\mathbf{D}_n|\mathbf{X}}$  is  $\sqrt{n}$  consistent for estimating the true central space of  $\mathbf{D}_n$  from the marginal central spaces of  $\mathcal{S}_{u^\top \mathbf{D}_n|\mathbf{X}}$  if  $N$  converges to  $\infty$  at a rate faster than  $n$ . Therefore, for any random response object  $Y$  in a compact metric space  $(\Omega_Y, d)$ , Lemma 1 and Theorem 2 guarantees the recovery of a consistent unbiased estimator for  $\mathcal{S}_{Y|\mathbf{X}}$ .

## 4 Simulation Experiments

In this section, we compare the performance of our proposed surrogate-assisted methods to other competing methods where possible on synthetic data. Let  $\mathbf{B}$  be the true basis of

$\mathcal{S}_{Y|\mathbf{X}}$  and  $\hat{\mathbf{B}}$  be the estimate of  $\mathbf{B}$ . For each method, we measure the estimation accuracy using

$$\Delta = \|\mathbf{P}_{\mathbf{B}} - \mathbf{P}_{\hat{\mathbf{B}}}\|_F, \quad (13)$$

where  $\mathbf{P}_{\mathbf{A}} = \mathbf{A}(\mathbf{A}^\top \mathbf{A})^{-1}\mathbf{A}^\top$  and  $\|\cdot\|_F$  is the matrix Frobenius norm. Smaller values of  $\Delta$  indicate better accuracy.

## 4.1 Euclidean response

Fix  $p \in \{10, 20\}$  and  $n \in \{100, 500\}$  and generate the predictor as  $\mathbf{X} \sim N(\mathbf{0}, \mathbf{I}_p)$ . Let  $\beta_1^\top = (1, 1, 0, \dots, 0)$ ,  $\beta_2^\top = (1, 0, \dots, 0)$ , and  $\beta_3^\top = (0, 1, 0, \dots, 0)$  with  $\beta_1, \beta_2, \beta_3 \in \mathbb{R}^p$ . Next, generate the response as follows:

$$\text{I. } Y = 0.5 + \sin(\beta_1^\top \mathbf{X}) + 0.5\epsilon$$

$$\text{II. } Y = (1 + \beta_1^\top \mathbf{X})\epsilon$$

$$\text{III. } Y = 0.5(\beta_2^\top \mathbf{X})^3 + (\beta_3^\top \mathbf{X} + 2)\epsilon,$$

where  $\epsilon \sim N(0, 1)$ . Model I is a standard homoscedastic error single-index model with  $\mathbf{B} = \beta_1$  and  $d = 1$ . Model II is the toy model illustrated in the motivation but with more predictors. For model III,  $\mathbf{B} = (\beta_2, \beta_3)$  and  $d = 2$  with heteroscedastic errors. We compare the classical OLS and SIR with their surrogate-assisted counterparts, sa-OLS and sa-SIR, respectively. The number of slices is fixed at 5 for both SIR and sa-SIR under all settings. The simulation results are provided in Table 1. All results are based on 500 random replicates.

In model I, because the central space depends on the direction in  $E(Y|\mathbf{X})$ , we expect the OLS to perform better than SIR under both the classical and surrogate-assisted technique as demonstrated in Table 1. However, for model II, because  $\mathcal{S}_{E(Y|\mathbf{X})} = \{\mathbf{0}\}$ , classical OLS performs abysmally. Unsurprisingly, this handicap is not shared by sa-OLS and it performs

Table 1: Mean (standard deviation) of  $\Delta$  based on 500 random repetitions.

Model	n	p	OLS	sa-OLS	SIR	sa-SIR
I	100	10	0.5206 (0.0070)	0.5096 (0.0071)	0.5465 (0.0075)	0.5448 (0.0077)
		20	0.7460 (0.0071)	0.7327 (0.0072)	0.7858 (0.0079)	0.7819 (0.0078)
	500	10	0.2396 (0.0028)	0.2321 (0.0028)	0.2402 (0.0029)	0.2402 (0.003)
		20	0.3577 (0.0030)	0.3462 (0.0029)	0.3568 (0.003)	0.3570 (0.003)
II	100	10	1.2791 (0.0072)	0.7686 (0.0095)	0.9391 (0.0107)	0.8183 (0.0103)
		20	1.3424 (0.004)	0.9902 (0.0078)	1.1585 (0.008)	1.0491 (0.0086)
	500	10	1.2655 (0.0071)	0.3814 (0.0046)	0.4482 (0.0052)	0.3806 (0.0046)
		20	1.3313 (0.0045)	0.5430 (0.0045)	0.6349 (0.0048)	0.5447 (0.0045)
III	100	10	NA	1.1855 (0.0088)	1.2340 (0.0091)	1.2323 (0.0091)
		20		1.4818 (0.0058)	1.5669 (0.0062)	1.5719 (0.0061)
	500	10	NA	0.6495 (0.0064)	0.5926 (0.0051)	0.5876 (0.0050)
		20		0.9292 (0.0059)	0.8580 (0.0047)	0.8580 (0.0047)

much better than both the classical SIR and sa-SIR, which are better equipped to handle such settings. sa-SIR also has a slight edge over the classical SIR. The classical OLS does not apply in model III as it can only recover a single direction. However, this restriction does not apply to sa-OLS, which is another advantage sa-OLS enjoys over the classical OLS.

As expected, all methods show consistency in large samples for fixed  $p$  but show less accuracy with an increase in  $p$  when we fix  $n$ , under all settings. Overall, the results in Table 1 demonstrate the superiority or at least noninferiority of the surrogate technique even in the Euclidean space.

## 4.2 Distributional response

For the univariate distributional response, we follow the data generation process used in Zhang et al. (2021). We fix  $p \in \{10, 20\}$  and  $n \in \{100, 500\}$ , and generate i.i.d. observations  $X_i \sim Unif(0, 1) \in \mathbb{R}^p$  for  $i = 1, \dots, n$ . Let  $\beta_1^\top = (1, 1, 0, \dots, 0)/\sqrt{2}$  and  $\beta_2^\top = (0, \dots, 0, 1, 1)/\sqrt{2}$ . Each response object  $Y_i, i = 1, \dots, n$  is generated as a sample in  $\mathbb{R}^m$  as follows:

- I.  $Y_i \in \mathbb{R}^{100}$  as i.i.d.  $Unif(0, |\beta_1^\top \mathbf{X}_i|)$ .
- II.  $Y_i \in \mathbb{R}^{100}$  as i.i.d.  $N(\beta_1^\top \mathbf{X}_i, 1)$ .
- III.  $Y_i \in \mathbb{R}^{100}$  as i.i.d.  $N[\mu_Y(\mathbf{X}_i), \sigma_Y(\mathbf{X}_i)]$ , where  $\mu_Y(\mathbf{X}_i) \sim N[\exp(\beta_1^\top \mathbf{X}_i), 0.25]$  and  $\sigma_Y(\mathbf{X}_i) = (\beta_2^\top \mathbf{X}_i)^2$ .
- IV.  $Y_i \in \mathbb{R}^{100}$  as i.i.d.  $N[\mu_Y(\mathbf{X}_i), \sigma_Y(\mathbf{X}_i)]$ , where  $\mu_Y(\mathbf{X}_i) \sim N[(0, (\beta_1^\top \mathbf{X}_i)^2]$  and  $\sigma_Y(\mathbf{X}_i) = (\beta_2^\top \mathbf{X}_i)^2$ .

Model I is a modification of **I-1** in Zhang et al. (2021) with uniform distributions instead of the normal. Model II is also a slight modification of model **I-3** but with the normal distributions depending on  $\mathbf{X}$  through the mean instead of the variance. It is important to note that in both models, the Wasserstein distances are directly bounded by  $|\beta_1^\top(\mathbf{X} - \tilde{\mathbf{X}})|$ , and are more likely to be sparse since the predictors are very similar. Models III and IV are also slight modifications of models **I-2** and **I-4** in Zhang et al. (2021), respectively. Here, we compare the Fréchet OLS and SIR of Zhang et al. (2021), which we denote respectively as fOLS and fsIR, with their respective surrogate-assisted counterparts sa-OLS and sa-SIR. Again, the number of slices is fixed at 5 for both fsIR and sa-SIR under all settings and the simulation results provided in Table 3 are based on 500 random replicates.

In Table 3, we see that sa-OLS completely dominates the rest of the methods in the single-index models I and II under all settings of  $(n, p)$ . sa-SIR also performs relatively

Table 2: Mean (standard deviation) of  $\Delta$  based on 500 random repetitions.

Model	n	p	fOLS	sa-OLS	fSIR	sa-SIR
I	100	10	0.1139 (0.0013)	0.0919 (0.0010)	0.1593 (0.0019)	0.1429 (0.0017)
		20	0.1833 (0.0016)	0.1480 (0.0013)	0.2577 (0.0023)	0.2310 (0.002)
	500	10	0.0485 (0.0005)	0.0390 (0.0004)	0.0649 (0.0007)	0.0595 (0.0007)
		20	0.0735 (0.0006)	0.0587 (0.0005)	0.0980 (0.0007)	0.0897 (0.0007)
II	100	10	0.1762 (0.0020)	0.1627 (0.0018)	0.2130 (0.0024)	0.1949 (0.0022)
		20	0.2742 (0.0022)	0.2510 (0.0020)	0.3397 (0.0028)	0.3079 (0.0025)
	500	10	0.0764 (0.0008)	0.0698 (0.0008)	0.0897 (0.0010)	0.0834 (0.0009)
		20	0.1143 (0.0008)	0.1048 (0.0008)	0.1335 (0.0010)	0.1243 (0.0009)
III	100	10	0.3521 (0.0045)	0.3340 (0.0041)	0.3408 (0.0036)	0.2866 (0.0025)
		20	0.6191 (0.0074)	0.5845 (0.0066)	0.6004 (0.0064)	0.4852 (0.0033)
	500	10	0.1447 (0.0013)	0.1422 (0.0013)	0.1306 (0.0011)	0.1180 (0.0010)
		20	0.2272 (0.0016)	0.2230 (0.0016)	0.2058 (0.0012)	0.1849 (0.0011)
IV	100	10	0.6599 (0.0067)	0.6825 (0.0071)	0.5980 (0.0060)	0.5771 (0.0060)
		20	0.9907 (0.0083)	1.0434 (0.0091)	0.8922 (0.0059)	0.8603 (0.0059)
	500	10	0.2828 (0.0032)	0.2907 (0.0032)	0.2561 (0.0027)	0.2488 (0.0027)
		20	0.4307 (0.0031)	0.4470 (0.0033)	0.3873 (0.0026)	0.3766 (0.0026)

better than the Fréchet SIR across the different scenarios in these models, but fSIR is very competitive, unlike fOLS. In models III and IV, however, we see that although both fOLS and sa-OLS can recover more than one direction, they are not as competitive as the SIR-based methods. Overall, sa-SIR does appear to be the best at capturing the dependence in both the mean and variance of the distributions.

### 4.3 Functional response

For this setting, we consider functional responses that depend on time only through their intercepts. The predictor effect is fixed across time. We set the number of repeated measurements to 30 for each response object, and generate the locations of the measurements  $t$  from  $Unif(0, 10)$ . Next, we fix  $p \in \{10, 20\}$  and  $n \in \{100, 500\}$ , and generate the fixed predictor  $\mathbf{X} \sim N(\mathbf{0}, \mathbf{I}_p)$ .

Let the time-varying intercept  $\alpha(t) = 10 \sin(\pi + \pi t/5)$  for  $t \in [0, 10]$  with  $|t| = 30$ . Let  $\beta_1^\top = (1, 1, 0, \dots, 0)/\sqrt{2}$  and  $\beta_2^\top = (0, \dots, 0, 1, 1)/\sqrt{2}$ . Lastly, generate the  $i$ th functional response  $Y_i(t)$  as follows:

- I.  $Y_i(t) = \alpha_0(t) + 2[\sin(\beta_1^\top \mathbf{X}_{1i})]\phi(t) + \epsilon_i(t),$
- II.  $Y_i(t) = \alpha_0(t) + [(\beta_1^\top \mathbf{X}_{1i})^3]\phi(t) + \epsilon_i(t),$
- III.  $Y_i(t) = \alpha_0(t) + 2[(\beta_1^\top \mathbf{X}_{1i})]\phi(t) + 0.5(\beta_2^\top \mathbf{X}_{1i})^3\epsilon_i(t),$

where  $\phi(t) = 1, \forall t$ , and  $\epsilon_i(t) \sim N(0, 1)$ . Note: here, a fixed predictor effect is added at each time point, which means we do not need to use  $\beta(t)$ .

Although sa-OLS performs slightly better than sa-SIR in Model I, the performance of both methods appears to be similar. Notice that this model is a standard homoscedastic model with a response mean linear in  $\mathbf{X}$ . In Model II, however, sa-SIR performs better, especially in large samples. Here, the response mean is not linear in  $\mathbf{X}$ . Model III is heteroscedastic but the response mean is linear in  $\mathbf{X}$ , and we see that sa-OLS again performs better than sa-SIR.

Table 3: Mean (standard deviation) of  $\Delta$  based on 500 random repetitions.

Model	n	p	sa-OLS	sa-SIR
I	100	10	0.3842 (0.0047)	0.4057 (0.0050)
		20	0.5807 (0.0053)	0.6064 (0.0055)
	500	10	0.1736 (0.0020)	0.1748 (0.0019)
		20	0.2546 (0.0020)	0.2600 (0.0021)
II	100	10	0.5703 (0.0096)	0.4590 (0.0057)
		20	0.8778 (0.0107)	0.6972 (0.0060)
	500	10	0.3016 (0.0071)	0.1952 (0.0022)
		20	0.4608 (0.0102)	0.2887 (0.0021)
III	100	10	1.1691 (0.0099)	1.3424 (0.0054)
		20	1.3478 (0.0052)	1.4314 (0.0025)
	500	10	1.0695 (0.0115)	1.2707 (0.0075)
		20	1.2258 (0.0077)	1.3640 (0.0037)

## 5 Analysis of COVID-19 transmissions in the U.S.

Coronavirus Disease 2019 (COVID-19) is a global pandemic that has wreaked havoc and continues to put stress on our daily interactions and health systems. The U.S. in particular has been severely affected by the pandemic in terms of the transmission rate and mortality associated with the virus. To gain a better insight into the transmission rate of COVID-19 in the U.S., the relationship between demographic characteristics and the distribution and trajectory of transmission rates across counties is investigated.

## 5.1 Data

Our response is the daily COVID-19 transmission rate per 100,000 persons, which is the reported change in the 7-day moving average of newly reported COVID cases for a given county in the U.S. between 08/1/2021 and 02/21/2022. The counties include all 50 States in addition to Puerto Rico and Washington DC, which are treated as independent “States” in this study. This data is publicly available from the Centers for Disease Control and Prevention (CDC) website (CDC (2023b)). As reporting varied vastly across the country, we restricted the data set to only counties with the maximum reported cases (189 repeated rates), whose histograms we were able to smooth to obtain probability density functions. Our final analysis sample consists of 1046 counties.

While there are many factors that could influence the transmission of COVID-19, we only focus on the county demographic characteristics that were stable across the study period and were not affected by local policy implementations such as mask mandates. The demographic data is obtained from the 2020 American Community Survey (ACS), which provides detailed information about the population and housing in communities across the country (US Census Bureau (2022)). Our predictor includes the following ten demographic characteristics: percentage of Non-Hispanic Blacks, percentage of Hispanics, percentage of adults 65 years and older, percentage of adults with no high school education, percentage of adults with a high school diploma, percentage of the population living below the poverty line, percentage of the labor force that is unemployed, percentage of renter-occupied homes, percentage of the population on public assistance programs, and the median household income. All predictors are marginally standardized before implementing SDR.

Our analysis considers two different scenarios. In the first case, we consider the distribution of County-level transmissions over the study period without any regard to the date of reporting. The second scenario considers the trajectory of case transmissions over time.

## 5.2 Distribution of transmissions as response

We illustrate the distributions of the county-level case transmission rates in six different counties across six different states in Figure 3. All the distributions appear to be right-skewed and peak at about 500 case transmissions per 100k persons. However, there is variation in the shapes of the distributions, which can be captured by the Wasserstein metric.

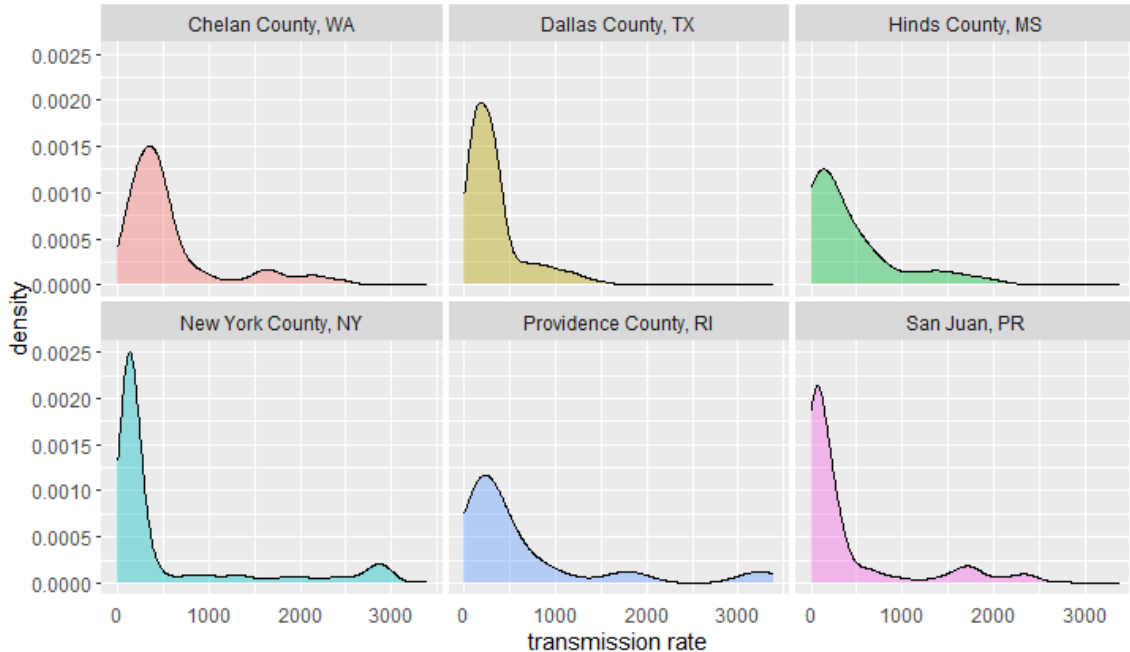


Figure 3: Distributions of COVID-19 case transmission rate across counties in the U.S. between 08/1/2021 and 02/21/2022.

Next, we smoothed the histograms of the transmission rates for each county to obtain probability density functions. This was done using the *Fréchet package* in *R*. The surrogate-assisted OLS and SIR and their Fréchet counterparts were then applied to the data. We determined the structural dimension  $d$  to be 1 based on the leading eigenvalues of the candidate matrices for all four methods. The estimated bases are given in Table 4.

Based on Table 4, the predictor that has the most influence on the distribution of transmis-

Table 4: estimated bases based on sa-OLS and sa-SIR

	fOLS	sa-OLS	fSIR	sa-SIR
% Non-Hispanic Blacks	0.2793	-0.0967	-0.8278	0.8710
% Hispanics	-0.1670	-0.1778	-0.1475	0.3982
% Adults 65+	-0.1650	0.1756	0.0647	0.0525
% No high school diploma	0.8692	0.7153	-0.2666	0.0336
% High school diploma	-0.2348	-0.6171	0.1337	-0.1225
% Living below poverty line	-0.1214	-0.5428	-0.2638	0.3704
% Unemployed	0.2260	-0.3434	-0.0357	0.0368
% Renter-occupied homes	-0.0123	0.0808	0.2522	-0.3184
% On public assistance	-0.0709	0.1222	0.2573	-0.2561
Median household income ('\$000)	-0.1643	-1.2262	-0.0919	0.0730

sion rate based on the Fréchet OLS estimate is the percentage with no high school diploma. The percentages of Non-Hispanic Blacks and unemployed also appear to have some slight effect on the distributions. For the sa-OLS estimate, we see that the most important predictor is median household income, but the percentage with a high school diploma or lower and those living in poverty also have a moderate influence on the transmission distributions. SIR-based estimates, i.e., fSIR and sa-SIR capture the percentage of Non-Hispanic Blacks to have the most important influence on the transmission rate distribution. They also captured slight contributions from the percentage living in poverty, renter-occupied homes, and public assistance. However, fSIR also captured the percentage with no High School diploma while sa-SIR captured the percentage of Hispanics.

We measured the consistency of the estimators by finding the stability measure  $\Delta_s = \|\mathbf{P}_{\mathbf{B}_C} - \mathbf{P}_{\hat{\mathbf{B}}_R}\|_F$ , where  $\mathbf{B}_C$  is the estimated basis based on the complete sample and  $\mathbf{B}_R$  is the estimated basis based on a reduced random sample, which is 60% of the full sample. For both OLS and SIR, the surrogate-assisted estimates appeared to be more stable compared

to their Fréchet counterparts.

Table 5: Mean (standard deviation) of  $\Delta_s$  based on 500 random repetitions.

	fOLS	sa-OLS	fsIR	sa-SIR
Mean	0.7922 (0.0091)	0.6830 (0.0136)	0.3909 (0.0055)	0.3631 (0.0053)

To gain more insights into the relationship between the distributions and the predictors, we visualize the plots between the distributions in our descriptive in Figure 3 and their corresponding sufficient predictors  $X\hat{\mathbf{B}}$  based on each method in Figure 4. We see that each sufficient predictor influences the distributions differently. For instance, Chelan County in Washington State has the highest peak based on the fOLS direction, but the lowest peak based on the sa-OLS direction. We also see that the spread and clustering of the distributions vary with each sufficient predictor.

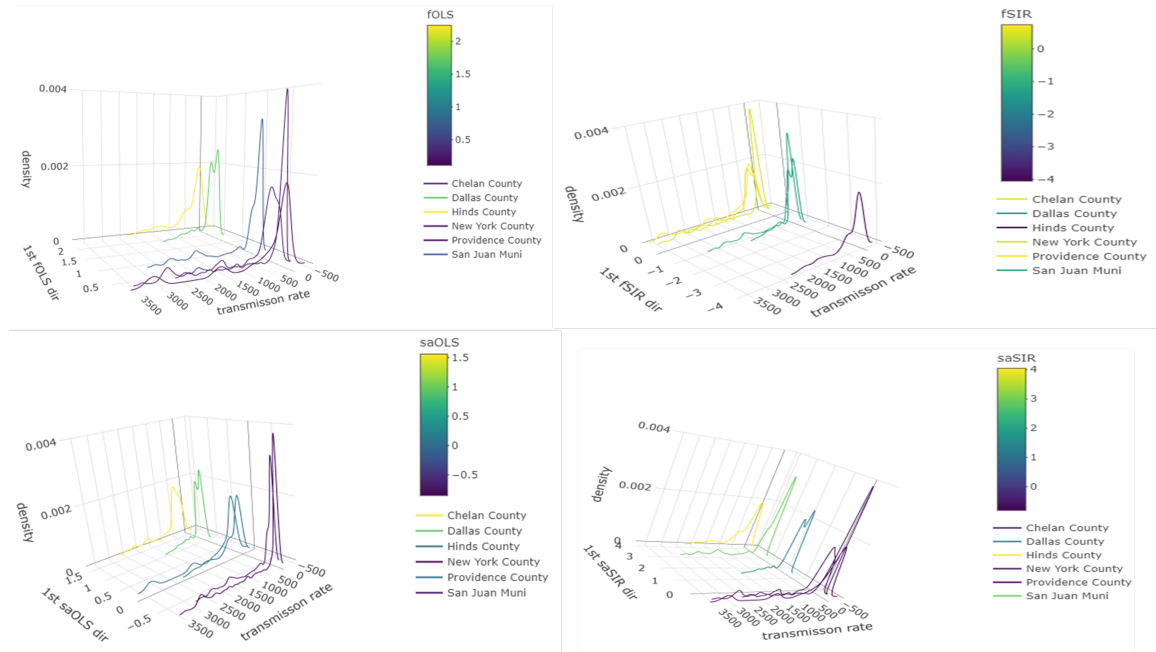


Figure 4: Plot of distributions of COVID-19 transmission rate vs sufficient predictors.

The advantage of regression with distributional responses is that we can explore the relationship between different aspects of the distributions and the sufficient predictor. The

plots of four summary statistics: mean, median, mode and standard deviation of transmission rates for all counties versus the first sufficient predictor based on sa-SIR are given in Figure 5. The variability in mean, median, and mode of the transmissions across counties appears to depend on the values of the first direction. The plot based on the standard deviations shows a clear outlier. We determined this outlier to be Covington County in Alabama. The takeaway is that counties with higher percentages of Non-Hispanic Blacks, Hispanics, people living in poverty and renter-occupied homes show more variability in the measures of the center of the transmission rates.

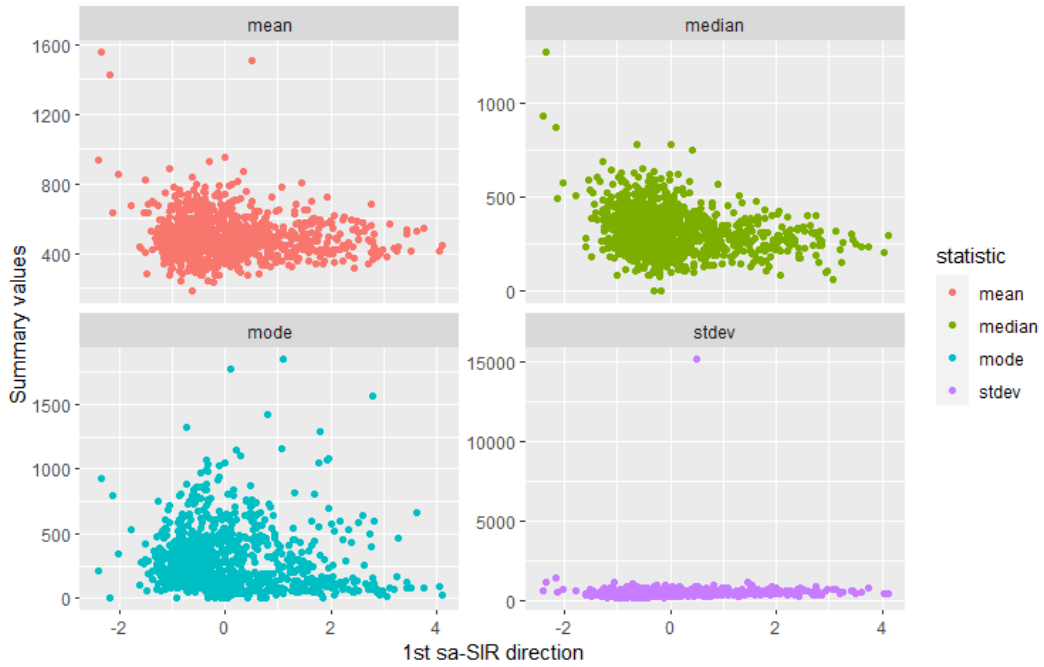


Figure 5: Scatter plot of some summary statistics of the distributions of COVID-19 transmission rate vs the first sufficient predictors based on sa-SIR.

### 5.3 Trajectory of transmissions over time as response

Here, we consider the time-dependent transmission rates for each county as the response of interest. Figure 6 gives the transmission rates over the 189-day study period across all study counties except Covington County, Alabama. The outlying observation is left out

for convenience to get a better view of the transmission rates across the 1,045 counties. In Figure 6, we see two peaks emerging around 30-45 days and 140-170 days. The first peak coincides with the first three weeks in September when the CDC announced an additional \$300 million and the Biden Administration invested \$2.1 billion in public health departments across the country to help increase testing and contain the spread. The second peak spans December 2021 through January 2022 which coincides with the emergence of the Omicron variant. By the first week of January 2022, the U.S. was reporting the highest daily total of any country in the world (CDC (2023a)). Outside these ranges, the transmission rate appears to be mostly stable with slight bumps.

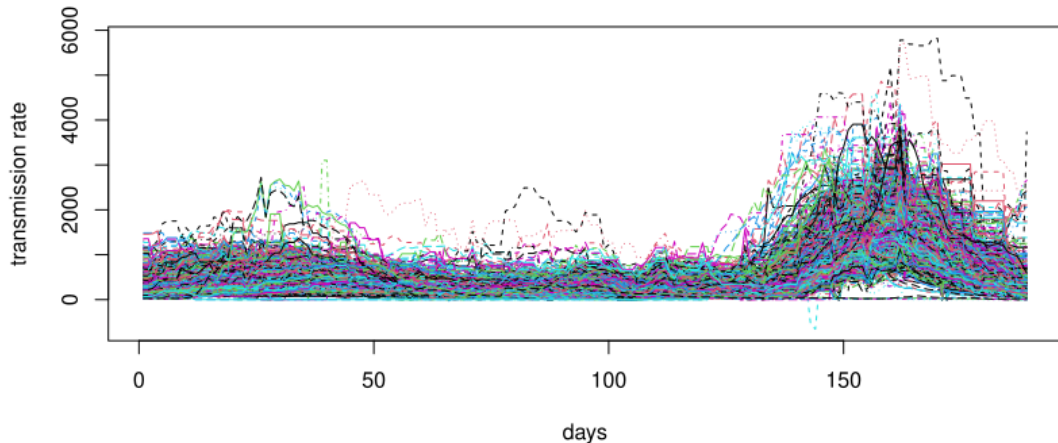


Figure 6: Daily reported COVID-19 transmission rates across counties in the U.S. between 08/1/2021 and 02/21/2022.

To investigate the effect of the predictors on the transmission rate trajectories, we apply the surrogate-assisted OLS and SIR. Again, we determined  $d = 1$  based on the eigenvalues of the candidate matrices for sa-OLS and sa-SIR. The estimated bases are given in Table 6. The directions of sa-OLS load heavily on the percentage of unemployed adults and moderately on the percentage of Non-Hispanic Blacks and Hispanics. For the sa-SIR directions, median household income and the percentage of Non-Hispanic Blacks

Table 6: estimated bases based on sa-OLS and sa-SIR

	sa-OLS	sa-SIR
% Non-Hispanic Blacks	-0.3327	-0.6112
% Hispanics	-0.3402	-0.3468
% Adults 65+	0.0500	-0.2524
% No high school diploma	0.1489	0.2569
% High school diploma	0.0609	-0.1789
% Living below poverty line	-0.0126	-0.0815
% Unemployed	1.0577	0.0379
% Renter-occupied homes	0.0064	-0.2390
% On public assistance	-0.2018	0.0624
Median household income ('\$000)	0.0326	-0.8674

have the most influence on the trajectory of transmissions over time. The percentage of Hispanics, adults 65+, no high school diploma, and those in renter-occupied homes also moderately influence the trajectory of transmissions. The sa-OLS and sa-SIR estimates differ from what we observed when we viewed the responses as distributions.

We take a deeper dive by fitting a functional-on scalar regression using the 1st sufficient predictors from sa-OLS and sa-SIR. We use 10 B-splines basis functions with knots at the reported days to obtain a smooth functional response and then separately regressed the functional response on each sufficient predictor. Both the sa-OLS and sa-SIR sufficient predictors were significantly associated with the average transmission rates. Overall, the County-level COVID-19 transmission is influenced more by determinants of income either in the form of the percentage of unemployed adults or median household income. The percentage of racial minorities, i.e., Non-Hispanic Blacks and Hispanics in the county also moderately influences the transmission trajectories. The predicted average transmission rates are given in Figure 7. All the functional regression analysis was implemented using

the *fda* package in *R*.

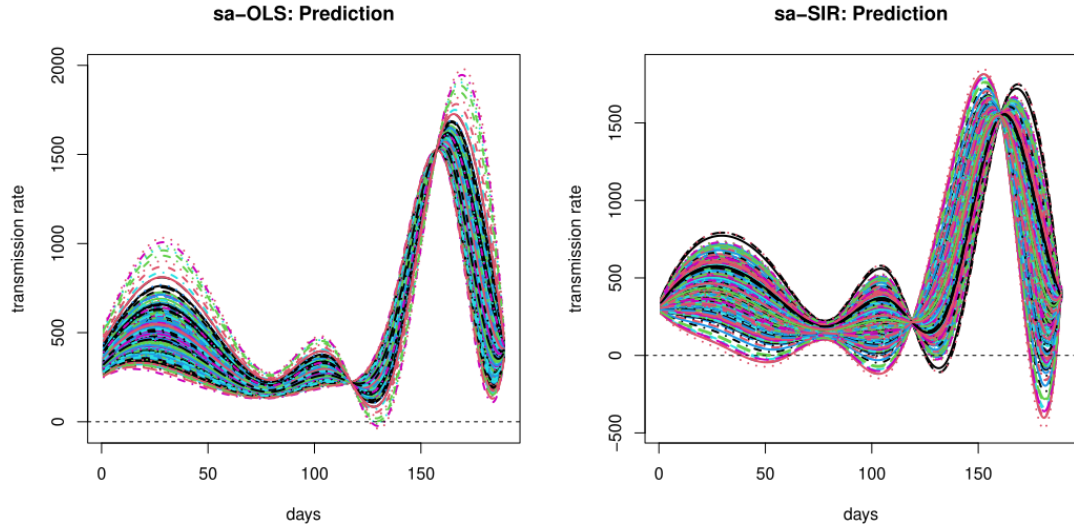


Figure 7: Predicted COVID-19 transmission rates based on the 1st sa-OLS and 1st sa-SIR predictors.

## 6 Discussion

This paper proposes a data visualization and dimension reduction technique for regressing metric-valued responses on Euclidean predictors, where the link function is monotonic. Adopting the projective resampling technique of Li et al. (2008) allows us to bypass the generation of high-dimensional universal kernels on the response space as proposed in Zhang et al. (2021). Although we only illustrated this idea for responses that are Euclidean, univariate distributions, and functional, our proposal readily extends to response objects that are multivariate distributions, positive definite matrices, graph Laplacians, and spheres, to mention a few. Regardless of the response type, the key is to use the appropriate metric to get the pairwise distances. For instance, for the space of positive definite matrices, the Frobenius metric may be used. In addition, the proposed method can be extended to other SDR methods such as the minimum average variance estimate (MAVE) and outer product

of gradient (OPG) and its extensions (Xia et al. (2002, 2009)).

Both the synthetic data in the simulations and real data analyses of COVID-19 transmissions demonstrate that the sa-OLS and sa-SIR are very powerful tools for visualization in regression settings with complex responses. These real analyses also make a strong case for dimension reduction methods that go beyond the Euclidean space as they give room to explore the relationship between different aspects of distributional, functional, and other repeatedly measured responses and the sufficient predictor. For instance, here we were able to see how different measures of the central tendency as well as the standard deviation of the COVID transmission rates vary with the first two sufficient predictors. On the contrary, if we were using the classical SDR methods, we would only be able to model a summary statistic of the transmission rates, say, the mean as a function of the demographics. But then, we may not gain any useful insights on how other statistics are influenced by the same factors.

Lastly, while being able to model a random response object as a function of Euclidean predictors expands our boundaries of applications, there is still room for more novel methods. For instance, it will be interesting to see how the distribution of the weekly transmission rate influences the distribution of the vaccination rate while controlling for other demographic factors. This will require techniques that can handle the regression of a random response on random predictor objects, which may include a mixture of predictor classes. In addition, the method illustrated in this paper covers only linear dimension reduction. An extension to nonlinear methods and non-monotone link functions will be an interesting domain to explore in the future.

## Acknowledgements

We thank the Children’s Environmental Health Initiative for helping us to organize the data on COVID-19 transmissions and the 2020 American Community Survey data.

## A Appendix of proofs

*Proof of Theorem 1.*

Suppose (a) does not hold. Then by the compactness of  $\mathcal{X}$  and continuity of  $f(\mathbf{X})$ , there exists a point  $\mathbf{X}_0$  such that  $\mathbf{X}$  and  $\mathbf{X}'$  converge to  $\mathbf{X}_0$  but  $d_Y/d_X \rightarrow \infty$ , which contradicts the initial claim that the spread  $s_f(\mathbf{X}_0)$  is finite. Next, assume (b) fails. Then for any  $\epsilon > 0$ , there exists a sequence of points  $\{c_i\}$  which converge to  $\mathbf{X}_0$  such that  $c_i \mathbf{X}_i \rightarrow 0$  and  $c_i \mathbf{X}'_i \rightarrow 0$ , but  $|s_f(\mathbf{X}_i) - d_Y/d_X| > 0$ . However, this contradicts the hypothesis that  $s_f(c_i) \rightarrow s_f(\mathbf{X}_0)$ , which concludes the proof.  $\square$

*Proof of Lemma 1.*

Let  $\mathcal{S}$  denote a sufficient dimension reduction space of the regression of  $Y$  versus  $\mathbf{X}$  and  $\mathfrak{F}$  be the collection of all subspaces for  $Y$  versus  $\mathbf{X}$ . Given a measurable function  $\psi$ , let  $\mathfrak{G}$  be the collection of all subspaces for  $\psi(Y)$  versus  $\mathbf{X}$ . By definition,  $Y \perp\!\!\!\perp \mathbf{X} | \mathbf{B}^\top \mathbf{X} \Rightarrow \psi(Y) \perp\!\!\!\perp \mathbf{X} | \mathbf{B}^\top \mathbf{X}$ , which implies  $\mathfrak{F} \subseteq \mathfrak{G}$ . Therefore,  $\bigcap \{\mathcal{S} : \mathcal{S} \in \mathfrak{F}\} \supseteq \{\mathcal{S} : \mathcal{S} \in \mathfrak{G}\}$ .  $\square$

*Proof of Lemma 2.*

The proof of (a) and (b) follows directly from Lemma 2.1 while that of (c) follows from Theorem 2.1 in Yin & Li (2011) and is thus omitted.  $\square$

*Proof of Theorem 2.*

The details of the proof of this theorem can be seen directly from Theorems 3.2 and 3.3 in Li et al. (2008).  $\square$

## References

Agrawal, R., Faloutsos, C. & Swami, A. (1993), Efficient similarity search in sequence databases, *in* ‘Foundations of Data Organization and Algorithms: 4th International Conference, FODO’93 Chicago, Illinois, USA, October 13–15, 1993 Proceedings 4’, Springer, pp. 69–84.

Bhattacharjee, S. & Müller, H.-G. (2021), ‘Single index Fréchet regression’, *arXiv preprint arXiv:2108.05437*.

CDC (2023a), ‘CDC Museum COVID-19 Timeline’. [Online; accessed 13-March-2023].

CDC (2023b), ‘United States COVID-19 County Level of Community Transmission Historical Changes’. [Online; accessed 13-March-2023].

Cook, R. D. (1996), ‘Graphics for regressions with a binary response’, *Journal of the American Statistical Association* **91**(435), 983–992.

Dong, Y., Soale, A.-N. & Power, M. D. (2022), ‘A selective review of sufficient dimension reduction for multivariate response regression’, *arXiv preprint arXiv:2202.00876*.

Dong, Y. & Wu, Y. (2022), ‘Fréchet kernel sliced inverse regression’, *Journal of Multivariate Analysis* **191**, 105032.

Faraway, J. J. (2014), ‘Regression for non-euclidean data using distance matrices’, *Journal of Applied Statistics* **41**(11), 2342–2357.

Fréchet, M. (1948), Les éléments aléatoires de nature quelconque dans un espace distancié, *in* ‘Annales de l’institut Henri Poincaré’, Vol. 10, pp. 215–310.

Ghosal, A., Meiring, W. & Petersen, A. (2023), ‘Fréchet single index models for object response regression’, *Electronic Journal of Statistics* **17**(1), 1074–1112.

Huber, P. J. (1985), ‘Projection pursuit’, *The annals of Statistics* pp. 435–475.

Li, B. (2018), *Sufficient dimension reduction: Methods and applications with R*, CRC Press.

Li, B., Wen, S. & Zhu, L. (2008), ‘On a projective resampling method for dimension reduction with multivariate responses’, *Journal of the American Statistical Association* **103**(483), 1177–1186.

Mori, U., Mendiburu, A. & Lozano, J. A. (2016), ‘Distance Measures for Time Series in R: The TSdist Package’, *The R Journal* **8**(2), 451–459.  
**URL:** <https://doi.org/10.32614/RJ-2016-058>

Panaretos, V. M. & Zemel, Y. (2019), ‘Statistical aspects of wasserstein distances’, *Annual review of statistics and its application* **6**, 405–431.

Petersen, A. & Müller, H.-G. (2019), ‘Fréchet regression for random objects with euclidean predictors’, *The Annals of Statistics* **47**(2), 691–719.

US Census Bureau (2022), ‘United States Census Bureau’, <https://www.census.gov/data.html>. Accessed: 2022-10-26.

Wilson, W. (1935), ‘On certain types of continuous transformations of metric spaces’, *American Journal of Mathematics* **57**(1), 62–68.

Xia, Y., Tong, H., Li, W. K. & Zhu, L.-X. (2002), ‘An adaptive estimation of dimension reduction space’, *Journal of the Royal Statistical Society. Series B (Statistical Methodology)* **64**(3), 363–410.

Xia, Y., Tong, H., Li, W. K. & Zhu, L.-X. (2009), An adaptive estimation of dimension reduction space, in ‘Exploration Of A Nonlinear World: An Appreciation of Howell Tong’s Contributions to Statistics’, World Scientific, pp. 299–346.

Yin, X. & Li, B. (2011), ‘Sufficient dimension reduction based on an ensemble of minimum average variance estimators’.

Yin, X., Li, B. & Cook, R. D. (2008), ‘Successive direction extraction for estimating the central subspace in a multiple-index regression’, *Journal of Multivariate Analysis* **99**(8), 1733–1757.

Zhang, Q., Xue, L. & Li, B. (2021), ‘Dimension reduction and data visualization for fréchet regression’, *arXiv preprint arXiv:2110.00467* .